Aeroacoustics Conferences
June 4-7, 2024, Rome, Italy
30th AIAA/CEAS Aeroacoustics Conference (2024)

10.2514/6.2024-3201

On the generation and propagation of guided jet waves

Petrônio A. S. Nogueira*
Monash University

André V. G. Cavalieri†
Instituto Tecnológico de Aeronáutica

Eduardo Martini‡
Institut Pprime-CNRS-Université de Poitiers-ENSMA

Aaron Towne§
University of Michigan

Peter Jordan¶
Institut Pprime-CNRS-Université de Poitiers-ENSMA

Daniel Edgington-Mitchell‖
Monash University

Upstream-travelling guided jet waves have been shown to be one of the key elements in many resonance processes underpinned in high-speed jets. Despite its importance, many of its characteristics, including how these waves are generated and how it can travel subsonically, have not been detailed in the literature. In this work, we aim to provide a clarification about the dynamics of this mode. With the aid of an acoustic scattering formulation, we are able to show that the guided-jet mode results from total-internal-reflection and transmission to decaying waves, arising from the shear layer behaving like a hard duct. After total reflection, only discrete streamwise wavenumbers may be supported by the flow, with these wavenumbers dictated by the fact that the standing wave formed inside of the jet must fit between the two shear layers. Close to the sonic line, the transmission of this mode to the outside is maximum, leading to a net-energy flux directed upstream, which dictates the direction of propagation of this mode in the eigenspectrum, providing a clear connection to the better understood soft-duct mode.

I. Introduction

Aeroacoustic resonances are present in a range of flow configurations associated with high-speed flight. These processes produce high-amplitude tones that may interact with the natural frequencies of aircraft components, potentially leading to structural failure (see, for instance Berndt [1]). Some of the most well-known aeroacoustic feedback processes are screech [2–4], impingement tones [5–9] and the more recently discovered high-subsonic jet resonance [10, 11]. Despite the complexity of the underlying turbulent flows in each of these processes, they can still be well described with very simple models such as the one proposed by Powell [2], which has four main stages: *(i)* the propagation of energy in the downstream direction; *(ii)* the conversion of this energy into an upstream-travelling wave; *(iii)* the upstream propagation of energy and; *(iv)* the conversion of this energy back into a downstream-travelling wave,

*Research Fellow, Department of Mechanical and Aerospace Engineering, Laboratory for Turbulence Research in Aerospace and Combustion, Monash University, Melbourne, Victoria 3800, Australia
†Associate Professor, Divisão de Engenharia Aeronáutica, Instituto Tecnológico de Aeronáutica, Praça Marechal Eduardo Gomes, 50, São José dos Campos, SP, Brazil
‡Associate professor, Département Fluides Thermique et Combustion, Institut Pprime-CNRS-Université de Poitiers-ENSMA, Chasseneuil du Poitou, Nouvelle-Aquitaine, France, 86360
§Assistant Professor, Department of Mechanical Engineering, University of Michigan, Ann Arbor, MI 48109, USA
¶Directeur de Recherche, Département Fluides Thermique et Combustion, Institut Pprime-CNRS-Université de Poitiers-ENSMA, Chasseneuil du Poitou, Nouvelle-Aquitaine, France, 86360
‖Associate Professor, Department of Mechanical and Aerospace Engineering, Laboratory for Turbulence Research in Aerospace and Combustion, Melbourne, Victoria 3800, Australia

closing the resonance loop. Though there are a broad range of aeroacoustic phenomena, this framework still captures a key element that must underpin any resonance process: the existence of two wave-like structures that can transport energy upstream and downstream.

In his early description of screech, Powell [2] identified the downstream- and upstream-travelling waves involved in resonance as being large-scale vortices and acoustic waves, respectively. These large-scale vortices have their origin in the Kelvin-Helmholtz instability, first studied by Rayleigh [12] and later explored by a number of researchers [13–15]. These vortices extract energy from the mean flow and grow exponentially for the first few diameters of the jet; as the shear layer thickens, the vortices become stable and start decaying as they travel in the streamwise direction. While early descriptions of resonance treated these vortices as discrete entities, it is now well established that a train of these vortices are best described as a single coherent structure called a *wavepacket* [16–18]. Since the work of Powell, significant effort has been expended in the study of this downstream-travelling structure, a structure which underpins a range of noise-generation phenomena [19–25]. The characteristics of wavepackets are generally well-predicted by linear-stability models; locally parallel models can predict the generation of these structures [17, 26, 27], spatial-marching methods can capture their growth and decay [18, 28–30], and even the modulation of the wavepacket by shocks within the flow can be predicted [31]. These wavepackets constitute the downstream component of both screech and impingement tones; in high-subsonic jet resonance, it is replaced by a downstream-travelling neutral duct-like mode, which is acoustic in nature [10].

The upstream component of the resonance loops has been the object of more debate. In screech and impingement tones, early works such as Wagner [6] and Powell [2] assume that the upstream propagation of energy takes the form of an acoustic wave generated by an interaction between the Kelvin-Helmholtz wavepacket and the shocks. This assumption went unchallenged for decades, until the works of Tam and Ahuja [32] and Tam and Norum [33]. Inspired by the inability of contemporary models to capture an experimentally observed Mach-number cut-off, the authors proposed that the feedback loop in impinging jets is closed by neutral discrete acoustic-like waves. These waves had been first identified in the linear stability calculations of Tam and Hu [34], inspired by experimental observations of Oertel [35]. The presence of these neutral waves and their role in impinging-jet resonance found empirical support in the numerical simulations of Gojon et al. [36]. A similar role for these waves in jet screech was suggested numerically and experimentally by Gojon et al. [37] and Edgington-Mitchell et al. [38], who showed that screech tones were only observed at frequencies where these discrete waves were neutrally stable. Further confirmation that this upstream wave is involved in the screech resonance loop was provided by Mancinelli et al. [39, 40], who demonstrated that predictions using the neutral wave were in better agreement with experimental data than predictions based on a model that assumed the upstream wave was purely acoustic. Finally, Nogueira et al. [41, 42] showed that screech is triggered by an absolute instability mechanism involving the Kelvin-Helmholtz mode and this upstream wave (which has recently been referred to as the *guided-jet mode*), and Edgington-Mitchell et al. [43] demonstrated that the upstream-travelling waves in these flows are almost always slower than the ambient speed of sound. In high-subsonic jet resonance, the characteristics of the guided-jet mode, including how it is supported by the flow and its interaction with other duct-like modes, is the actual mechanism that drives resonance; this mechanism has also been studied by a number of recent works [44–46]. In supersonic impinging jets, it has been shown that free-stream acoustic waves seem to be relevant in the resonance loop at some conditions [47], while others seem to be governed by the guided-jet mode [48].

Despite the plethora of evidence for the role of the guided-jet mode in resonance and the predictive power of models that incorporate it, the exact nature of this wave has remained something of an enigma. The wave travels with phase velocities lower than the sound speed, yet it appears to find its genesis in the continuous acoustic branch of the linearised Navier-Stokes spectrum [10]. Should this wave then be referred to as an "acoustic" wave? Results from Tam and Hu [34] and Edgington-Mitchell et al. [38] suggest that the wave must be acoustic in nature, but how then to explain the subsonic phase velocity, both predicted by theory and observed in experiment? An additional complication is that the guided-jet mode is only predicted to be neutrally stable for a finite band of frequencies and wavenumbers, yet free-stream acoustic waves can exist at all frequencies. Lastly, the guided-jet mode exhibits behaviour that is difficult to reconcile with simple free-stream acoustic waves; interactions between this wave and downstream-propagating duct-like waves produce saddle points in the complex-valued eigenspectra predicted by linear stability theory.

The purpose of this paper is thus to determine the nature of this important but enigmatic "guided-jet mode". Given the role it plays in a range of noise-generating jets, a better understanding of its theoretical underpinnings may be critical in the mitigation of sound produced by high-speed shear flows. Given the similarities between these modes and the duct-like modes analysed in Towne et al. [10], one could hypothesise that internal reflections is one of the driving dynamics of this wave. To confirm this, in an attempt to reconcile the acoustic properties it possesses with its subsonic phase velocity, the guided-jet mode will be considered in the context of an acoustic-scattering problem, as

suggested by Martini et al. [49]. The acoustic-scattering framework is well established, but has not yet been applied to the study of this particular flow structure. As will be seen, considering the problem from this perspective will both provide insight into the nature of the guided-jet mode and also provide explanations for much of the behaviour predicted by linear-stability theory. The paper is divided as follows: in section II the mathematical formulation of the acoustic-scattering problem and vortex-sheet model are presented. After that, results of scattering are shown and compared with the overall behaviour of the guided-jet mode predicted from the vortex-sheet dispersion relation in section III. Section IV provides an explanation for the direction of propagation of the guided-jet mode based on the acoustic energy flux, and the main conclusions of the analysis are then reviewed in section V.

II. Mathematical formulation

Most of this work is based on the two-dimensional Cartesian linearised compressible Euler equations in the frequency-wavenumber domain. As will be seen in the next sections, the planar problem allows for a more detailed exploration than the cylindrical one, but the conclusions will later be extended to round jets. As in previous works [13, 49], the mean velocity is considered to only have a non-zero component in the streamwise direction, and all quantities are normalised by the free-stream sound speed c_∞, specific volume v_∞ and a length h (which was chosen here to be the distance between the two shear layers in the case of a planar jet). Under these assumptions and normalisation, the governing equations reduce to

$$-\mathrm{i}\omega\nu + \mathrm{i}\alpha U\nu + \nu\frac{\partial\overline{\nu}}{\partial y} - \overline{\nu}(\mathrm{i}\alpha u + \frac{\partial v}{\partial y}) = 0, \tag{1}$$

$$-\mathrm{i}\omega u + \mathrm{i}\alpha U u + \nu\frac{\partial U}{\partial y} + \mathrm{i}\alpha\overline{\nu}p = 0, \tag{2}$$

$$-\mathrm{i}\omega v + \mathrm{i}\alpha U v + \overline{\nu}\frac{\partial p}{\partial y} + \nu\frac{\partial P}{\partial y} = 0, \tag{3}$$

$$-\mathrm{i}\omega p + \mathrm{i}\alpha U p + \nu\frac{\partial P}{\partial y} + \gamma P(\mathrm{i}\alpha u + \frac{\partial v}{\partial y}) = 0, \tag{4}$$

$$\tag{5}$$

where U, P and $\overline{\nu}$ are the mean streamwise velocity, pressure and specific volume, and (ν, u, v, p) are the fluctuations of specific volume, streamwise and normal velocity, and pressure respectively [10]. The pairs (ω, α) are the perturbation frequency and wavenumber, following the normal-mode ansatz, which assumes each component of the flow disturbances to have the form $\tilde{q}(x, y, t) = q(y)\exp(-\mathrm{i}\omega t + \mathrm{i}\alpha x)$. The system (1) - (4) may be further simplified by dividing the flow into separate domains, each of which is assumed to have a constant velocity – this constitutes one of the main simplifications of the vortex-sheet model, as developed by Lessen et al. [13]. Following this simplification, after some further algebra, one may obtain

$$\left[\frac{\mathrm{d}}{\mathrm{d}y^2} - \alpha^2 + \frac{(\omega - \alpha M_{i,o})^2}{T_{i,o}}\right] p_{i,o} = 0, \tag{6}$$

where $M = U/c_\infty$ is the acoustic Mach number, T is the temperature ratio (which is simply the ratio between ν in the different regions for an ideal isobaric jet) and the subscripts $_{i,o}$ are associated with the different regions of the jet (i for the inner (flow) region, and o for the outer (quiescent) region). Considering a jet discharged into a medium at rest, these parameters reduce to $M_o = 0, T_o = 1, M_i = M$ and $T_i = T$. Even though the resulting equation is dependent on the temperature ratio, this work will focus on isothermal jets, as the fundamental features of the guided-jet mode are basically independent of that parameter. This is the same equation solved by Lessen et al. [13] and Martini et al. [49] for the double vortex-sheet (DVS) problem.

The general solution of (6) is given by

$$p_{i,o}(y) = A_{i,o}\mathrm{e}^{\gamma_{i,o}y} + B_{i,o}\mathrm{e}^{-\gamma_{i,o}y}, \tag{7}$$

where

$$\gamma_{i,o} = \mathrm{i}\sqrt{\frac{(\omega - \alpha M_{i,o})^2}{T_{i,o}} - \alpha^2}. \tag{8}$$

Note that the branch cut was chosen such that $\mathrm{Im}(\gamma_{i,o}) \geq 0$. As will be seen shortly, the coefficients $A_{i,o}$, $B_{i,o}$ define the amplitudes of incoming/outgoing waves when $\mathrm{Re}(\gamma_{i,o}) = 0$. When $\mathrm{Re}(\gamma_{i,o})$ is non-zero, the appropriate coefficient is set to zero to ensure bounded disturbances far from the vortex-sheet. The coefficients in the different parts of the domain, $A_{i,o}$ and $B_{i,o}$, may be obtained after consideration of the symmetry of the problem and the relevant boundary and matching conditions. In the following sections, (7) and (8) will be solved in the form of an acoustic-scattering problem for a single vortex sheet (SVS) in Section II.A and in the form of linear stability problems for a planar double-vortex-sheet in Section II.B. One of the main advantages of the scattering formulation is the fact that the problem may be discussed in terms of incident, reflected and transmitted waves, which brings an element of causality that is absent in all eigen-analyses of these flows – the resulting wave will be a function of the characteristics of the incident one. A sketch of the different formulations with their respective characteristic inputs and outputs is shown in figure 1.

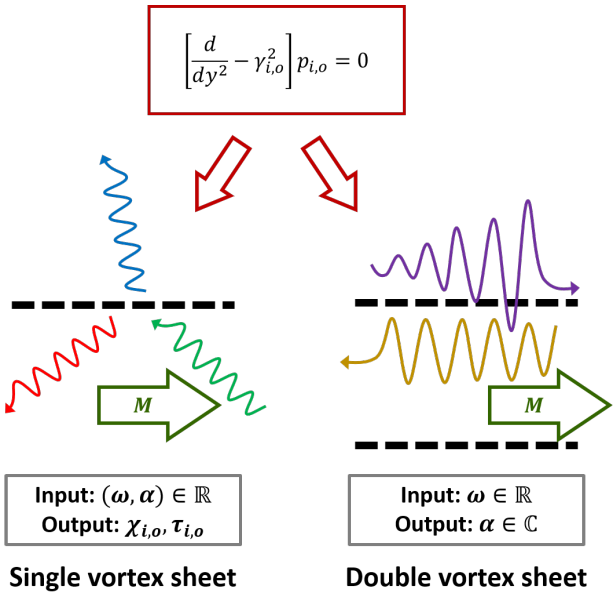

Fig. 1 Sketch of the different models considered in this work.

A. The acoustic scattering problem - single vortex sheet

The formulation presented in (7) may be used to study the problem of acoustic waves reflected by and transmitted through the shear layer in the SVS. This problem will be divided into two parts: *(i)* the scattering of waves coming from the quiescent region into the SVS; *(ii)* the scattering of waves coming from the flow region into the SVS. A sketch with the two configurations is provided in figure 2.

1. The scattering of waves generated in the quiescent region

For waves originating in the quiescent region, following Campos and Kobayashi [50], the resulting pressure field in the quiescent region contains contributions from both the incident and reflected waves, as given by

$$p_o(y) = \chi_o \mathrm{e}^{\gamma_i y} + \mathrm{e}^{-\gamma_i y} \ (y > 0), \tag{9}$$

while in the flow region, only transmitted waves exist

$$p_i(y) = \tau_o \mathrm{e}^{-\gamma_i y} \ (y < 0). \tag{10}$$

Here, the numbers χ_o and τ_o are the complex-valued reflection and transmission coefficients for this problem. Without loss of generality, incident waves will have unit amplitude $\iota = 1$ in this problem; the other coefficients are then obtained as ratios of ι. In order to calculate the resulting reflection and transmission coefficients, pressure and displacement must be matched at the vortex-sheet position, resulting in the following expression for the outer scattering problem in the SVS,

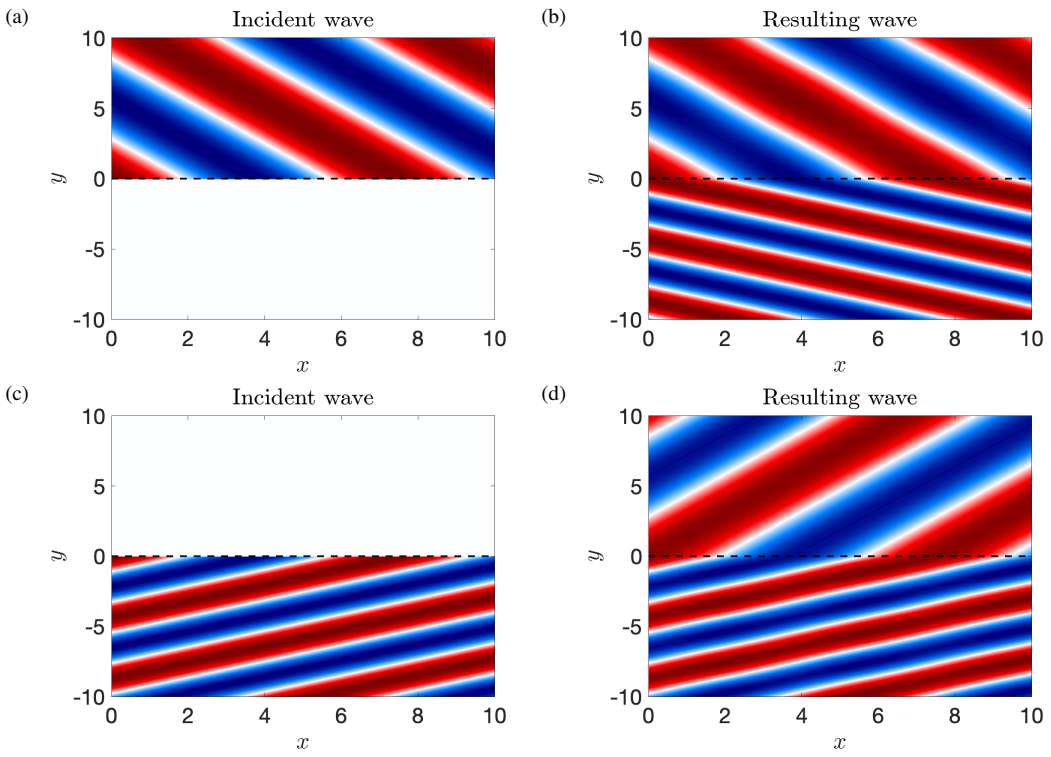

Fig. 2 Sample pressure fields associated with the scattering of waves coming from the quiescent region into the SVS (a,b) and the scattering of waves coming from the flow region into the SVS (c,d). Both incident (a,c) and resulting (b,d) pressure are shown. Note that the amplitudes of the reflected waves are small in these cases.

$$\chi_o = -\frac{1 - E_{SVS}}{1 + E_{SVS}}, \tag{11}$$

$$\tau_o = \chi_o + 1, \tag{12}$$

with

$$E_{SVS} = \left(1 - \frac{\alpha M}{\omega}\right)^2 \frac{1}{T} \frac{\gamma_o}{\gamma_i}. \tag{13}$$

Note that the expression for the reflection coefficient χ_o is similar to the one obtained for a wave incident on an impedance wall [51], in which case E_{SVS} may be interpreted as an impedance term. As we are dealing with acoustic waves that are oscillatory in the quiescent medium, the wavenumbers in (13) should be real-valued and restricted to $|\alpha| \leq \omega$. This is equivalent to defining the branch cut of the square-root function so as to obtain bounded disturbances at infinity. One should note that, in this range of wavenumbers, both γ_i and γ_o are pure imaginary numbers; thus E_{SVS} is a real number, leading to real transmission and reflection coefficients.

It is possible to include the edge of a plate or nozzle at the origin of the shear layer [52], which couples the acoustic scattering problem with the Kelvin-Helmholtz instability of the shear layer in order to satisfy an unsteady Kutta condition at the edge. This is not carried out here, for consistency with the local stability problem which does not include the edge.

2. The scattering of waves generated in the flow region

The scattering problem for waves coming from the flow region is similar, but requires more care; waves that are oscillatory in the flow region may not be oscillatory in the quiescent region. The opposite does not occur for negative wavenumbers, rendering the quiescent region analysis more straightforward. Again considering only waves that are

oscillatory in the quiescent medium ($|\alpha| \leq \omega$), the pressure field in this quiescent medium contains only transmitted waves, as given by

$$p_o(y) = \tau_i e^{\gamma_o y} \ (y > 0), \tag{14}$$

whereas the pressure field in the flow region contains both incident and reflected waves:

$$p_i(y) = e^{\gamma_i y} + \chi_i e^{-\gamma_i y} \ (y < 0). \tag{15}$$

Note that both transmitted and incident waves have the same exponential sign, ensuring that transmitted waves travel away from the vortex sheet. This is valid for incident waves with phase velocities in y pointing upwards, which is the case in the present work. The appropriate exponential sign may also be obtained by analysing the sign of the the group velocity in y. Furthermore, for $|\alpha| \leq \omega$, all disturbances are bounded as the parameters $\gamma_{i,o}$ are pure imaginary numbers. Implementing the same boundary conditions of matched pressure and displacement leads to the reflection and transmission coefficients

$$\chi_i = \frac{1 - E_{SVS}}{1 + E_{SVS}}, \tag{16}$$

$$\tau_i = \chi_o + 1. \tag{17}$$

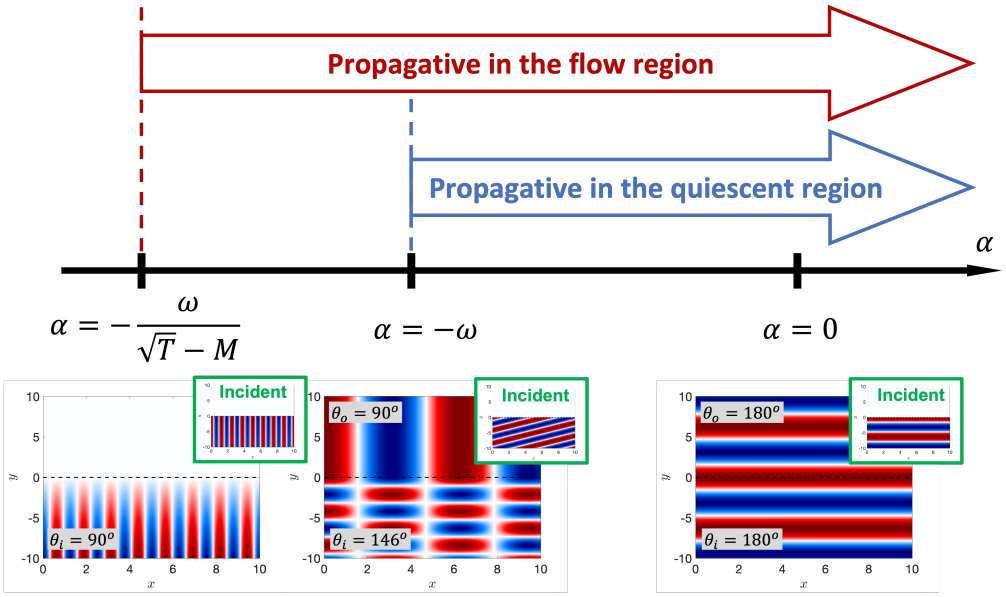

Fig. 3 Sketch showing the wavenumbers associated with oscillatory waves in the different regions of the flow and the propagation angles in the limit cases.

These expressions are valid for $|\alpha| \leq \omega$, but acoustic waves in the flow region exist for all wavenumbers in the interval $\frac{(\omega - \alpha M)^2}{T} - \alpha^2 > 0$. Thus, for subsonic flows and negative wavenumbers, there is an interval $\frac{-\omega}{\sqrt{T}-M} \leq \alpha < -\omega$ in which waves are oscillatory in the flow region and decaying in the quiescent region. The upper and lower limits of this interval are associated with oscillatory waves in the quiescent region travelling at 90° in the quiescent medium (but travelling at an angle in the flow medium), and travelling at 90° in the flow region (but decaying in the quiescent medium) with respect to the shear layer, respectively. This is shown schematically in figure 3. In this interval, the pressure for $y > 0$ is given by

$$p_o(y) = \tau_i e^{-\gamma_o y} \ (y > 0) \tag{18}$$

to ensure bounded pressure in both parts of the domain. Then, the reflection coefficient is given by

Wave Origin	$p_o(y)$	$p_i(y)$	χ
Quiescent	$\chi_o e^{\gamma_i y} + e^{-\gamma_i y}$	$\tau_o e^{-\gamma_i y}$	$\chi_o = -(1 - E_{SVS})/(1 + E_{SVS})$
Flow	$\tau_i e^{\pm\gamma_o y}$	$e^{\gamma_i y} + \chi_i e^{-\gamma_i y}$	$\chi_i = (1 \pm E_{SVS})/(1 \mp E_{SVS})$

Table 1 Summary of the different expressions for the scattering problem.

$$\chi_i = \frac{1 + E_{SVS}}{1 - E_{SVS}}. \tag{19}$$

Note that plane waves generated in the flow region must be written in the framework moving with the jet, which is already considered by the Doppler-shifted frequency in γ_i. Thus, the phase velocity of plane waves parallel to the y-axis (travelling directly upstream) match the speed of sound c in the quiescent medium; waves parallel to the same axis in the flow medium travel at speed $M - c$ (in the isothermal case), due to the convection by the mean flow. A summary of the different expressions for the scattering problem is shown in table 1.

B. The linear stability problem - double vortex-sheet

The dispersion relation for the DVS formulation as derived by Lessen et al. [13] is reviewed here for clarity. The governing equation is given by (6), whose solution is of the form (7). Taking the symmetry of the problem into account, one may simplify the expression for the pressure field as

$$p_o(y) = A\, e^{-\gamma_o y} \ (y > 0.5), \tag{20}$$

$$p_o(y) = \pm A\, e^{\gamma_o y} \ (y < -0.5), \tag{21}$$

and

$$p_i(y) = e^{\gamma_i y} \pm e^{-\gamma_i y} \ (|y| < 0.5), \tag{22}$$

where the parameter A in (20) may be obtained by matching the pressure solutions at the interface between the two media. The dispersion relation is then obtained by imposing that the displacement of the vortex sheet be the same in both sides, as in Lessen et al. [13]. These boundary conditions are the same as those imposed in the acoustic scattering single vortex sheet, though the consideration of problem symmetry results in different coefficients for the pressure fields. The amplitude ratio is

$$A = \frac{e^{\gamma_i/2} \pm e^{-\gamma_i/2}}{e^{-\gamma_o/2}}, \tag{23}$$

and the dispersion relation may be written as

$$\frac{1}{T}\left(1 - \frac{\alpha M}{\omega}\right)^2 + \frac{\gamma_i}{\gamma_o}\left(\frac{e^{\gamma_i/2} \mp e^{-\gamma_i/2}}{e^{\gamma_i/2} \pm e^{-\gamma_i/2}}\right) = 0. \tag{24}$$

The equation above may be used to obtain the frequency and wavenumber pairs of the waves supported by the flow in the limit of a very thin shear layer. The pressure eigenfunctions are then obtained using (20), (21) and (22). This formulation supports Kelvin-Helmholtz, duct-like and guided-jet modes, as studied in Martini et al. [49], being the Cartesian equivalent of the formulation used in Towne et al. [10] and Jordan et al. [53].

III. Transmission and reflection of acoustic waves in a single vortex sheet

Given that the guided-jet mode shares several, but not all, attributes of free-stream acoustic waves, it could be expected that this mode may be the consequence of reflection and transmission of acoustic waves. It has been shown in Towne et al. [10] that the duct-like mode is dictated by a total reflection, and Martini et al. [49] showed that this is due to a vanishing vortex-sheet impedance for large α. A natural departure point for this study is a consideration of how planar acoustic waves are scattered by a shear layer, as a function of their origin and angle of incidence. The same

problem has been analysed by a number of prior authors [50, 52, 54–57], but it is useful to review some of these results here, and particularise them for the case of an upstream-travelling wave. Waves that are generated outside of the flow are discussed first, then waves that are generated within it. Note that many times these waves will be categorised as *oscillatory* or *decaying*; these labels refer specifically to the behaviour of these waves in the y direction. Decaying then refers to exponentially decaying wave-shapes in y, and oscillatory refers to a oscillatory (cosine-like) shape in that direction. These are also denoted *propagative* and *evanescent* waves in the acoustics literature [see, for instance, 51], but we choose to adopt an alternative nomenclature as to avoid confusion with stable/unstable waves in the x-direction.

A. Waves generated in the quiescent region

Let us first consider the case of an acoustic wave generated in the quiescent region ($y > 0$), where there is no flow. For an acoustic wave travelling upstream, the limits of the analysis are $-\omega \leq \alpha \leq 0$; this range of wavenumbers span all possible angles of incidence from 90° to 180°. As we are most interested in building a model for the guided-jet mode, the most interesting parts of the analysis are obtained when the wavenumber of the wave is close to sonic $c = -1$ (when the quiescent waves are almost aligned with the VS); however, for completeness, the following plots will be restricted to a minimum phase velocity $c = \omega/\alpha = -10$. Figure 4 shows the imaginary part of the coefficients $\gamma_{i,o}$, which may be interpreted as the wavenumber of the waves in the y-direction. In this interval, the waves are oscillatory in both streams (the real part of the coefficients are zero), leading to a purely oscillatory behaviour in both regions of the domain. As the phase velocity tends to -1, the coefficient γ_o tends to zero – this is the limit in which the outer wave travels in a direction opposite to the flow. However, even at this limit, γ_i is still a purely imaginary number, leading to a transmitted wave that is oscillatory in the flow region. The angles of propagation (calculated as $\theta_{i,o} = \text{atan}(\alpha/\gamma_{i,o})$) are shown in the same figure. As expected, the incidence angle ranges from $\theta_o = 180°$ (waves travelling directly towards the shear layer, in the limit $c \to -\infty$) to $\theta_o = 90°$, (waves travelling directly upstream), as shown schematically in figure 3. The angle of the transmitted wave has a somewhat slower variation, starting at $\theta_i = 180°$ at $c \to -\infty$, and reaching $\theta_i \approx 146°$ for this case.

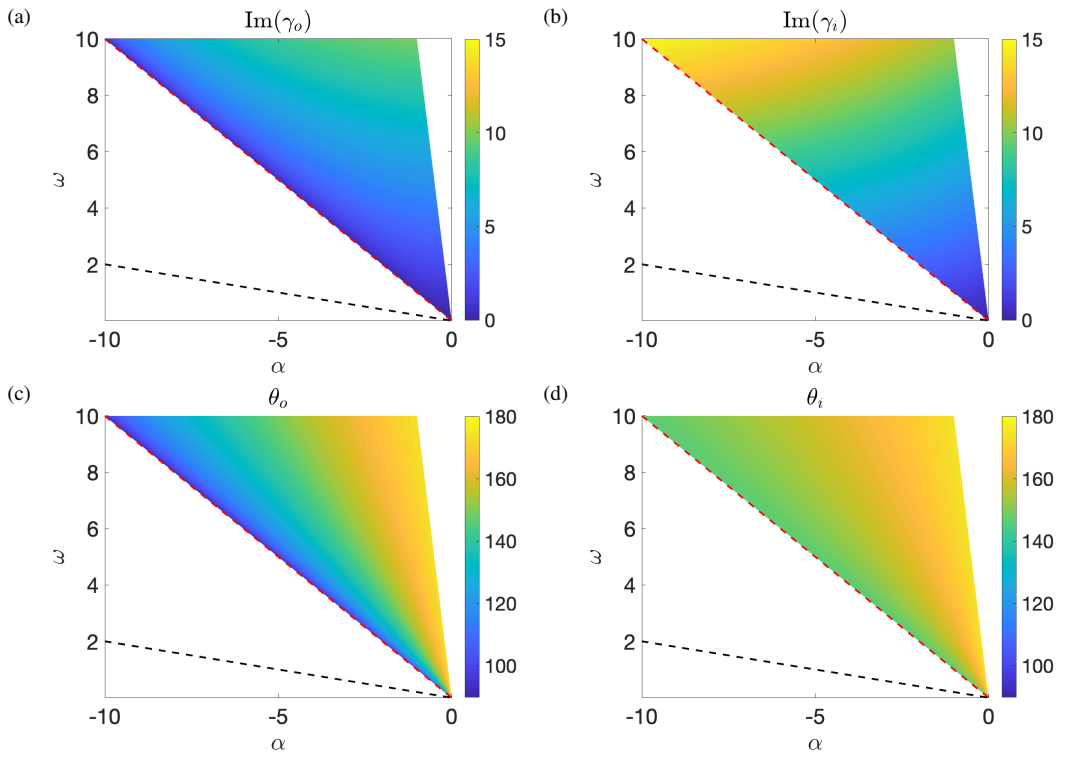

Fig. 4 Imaginary part of the coefficients $\gamma_{i,o}$ and their associated propagation angle for upstream-travelling waves generated in the quiescent region. Red dashed lines: $\alpha = -\omega$. Black dashed lines: $\alpha = -\omega/(\sqrt{T} - M)$. Results for $M = 0.8, T = 1$.

The preceding analysis of the angles of propagation elucidates the behaviour of the transmitted wave as a function of the incidence angle, but it does not reveal anything about the amplitude of the reflected and transmitted waves; amplitude information is only contained in the coefficients χ and τ. The coefficients are shown in figure 5. These plots display two noteworthy features. The first is that there is a value of incidence angle for which all waves are transmitted and there is no reflection – the frequency-wavenumber pairs associated with zero reflection are also a solution of the SVS dispersion relation. Perhaps more interesting is the fact that the transmission coefficient tends to zero as c tends to -1 (or as θ_o tends to 90°); this also leads to a reflection coefficient of -1, meaning that incident and reflected waves are in perfect phase opposition. Substitution of these values into (9) and (10) results in a complete cancellation of the wave by the scattering. Critically, this result demonstrates that planar waves travelling directly upstream cannot be transmitted to the flow region, at least under the hypotheses of this simplified model. Thus, if the waves originate from the quiescent region, there is no linear mechanism in which a planar wave travelling parallel to the stream produces pressure disturbances in the flow region. This result suggests that though the guided-jet mode shares some properties with free-stream acoustic waves, it cannot simply be interpreted as the signature of an upstream-travelling acoustic wave interacting with the flow. The guided-jet mode is characterised by higher-magnitude pressure fluctuations within the jet core than external to it; the preceding analysis demonstrates this cannot arise due to the transmission of a wave generated outside the flow.

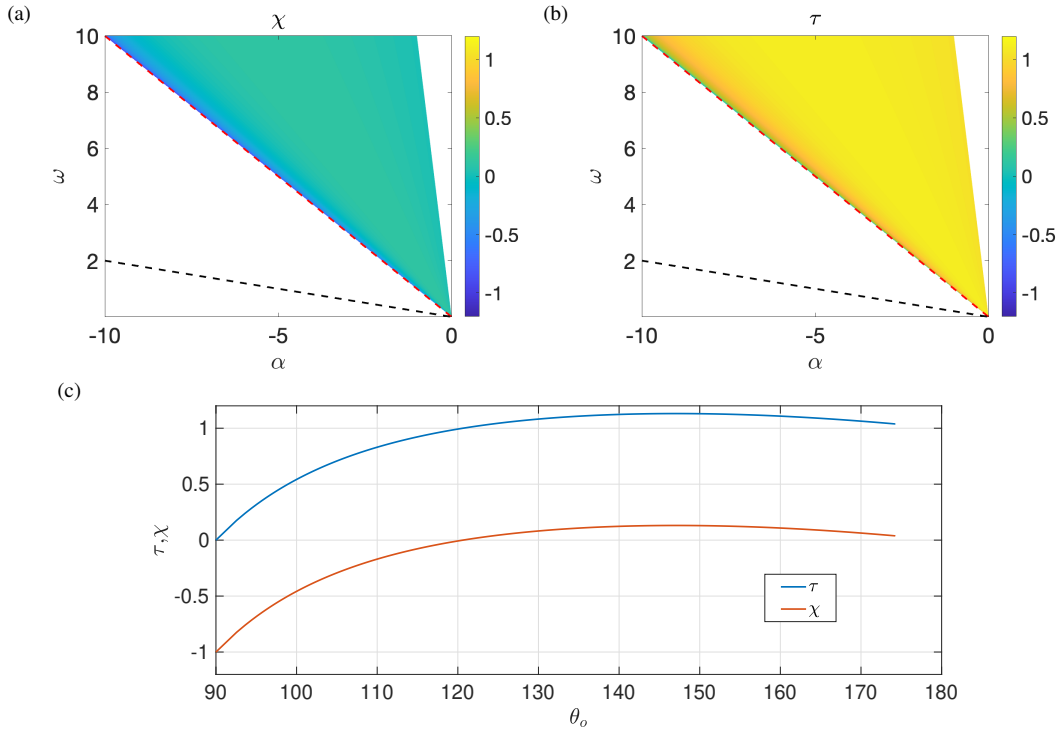

Fig. 5 Reflection and transmission coefficients for upstream-travelling waves generated in the quiescent region $M = 0.8$ and $T = 1$. Coefficients shown as a function of α and ω (a,b) and as a function of the quiescent medium wave incidence angle θ_o. Red dashed lines: $\alpha = -\omega$. Black dashed lines: $\alpha = -\omega/(\sqrt{T} - M)$.

B. Waves generated in the flow region

Let us now analyse a similar problem, but with waves generated in the flow region. As in the previous case, these waves will be transmitted and reflected by the shear layer; the difference now is that the transmitted wave may also be decaying, which could not occur in the previous case. Figure 6 shows the values of $\gamma_{i,o}$ as a function of α for all the allowable angles of incidence in the flow region (the angles that correspond to oscillatory waves in that region), and the respective resultant angles. Red dashed lines indicate the wavenumbers of an acoustic wave travelling upstream in the quiescent region ($\alpha = -\omega$) and black dashed lines indicate the wavenumbers associated with a wave travelling directly upstream in the flow region ($\alpha = -\omega/(\sqrt{T} - M)$). It is clear that, between these two lines, the imaginary part of γ_o is

zero, leading to waves that travel at 90° in that part of the domain for a range of incidence angles. As both frequency and wavenumber are real in (8), this also means that γ_o is a real number; thus, following (7), this wave is exponentially damped in y for these angles. Also, even though this wave is travelling at sonic speeds in the flow region [see 55], it is effectively subsonic in the quiescent region when the transmission leads to decaying waves in the quiescent medium. In the higher limit ($\alpha = -\omega$), the wave travels at the speed of sound in x, but has supersonic phase velocity in x in the flow medium.

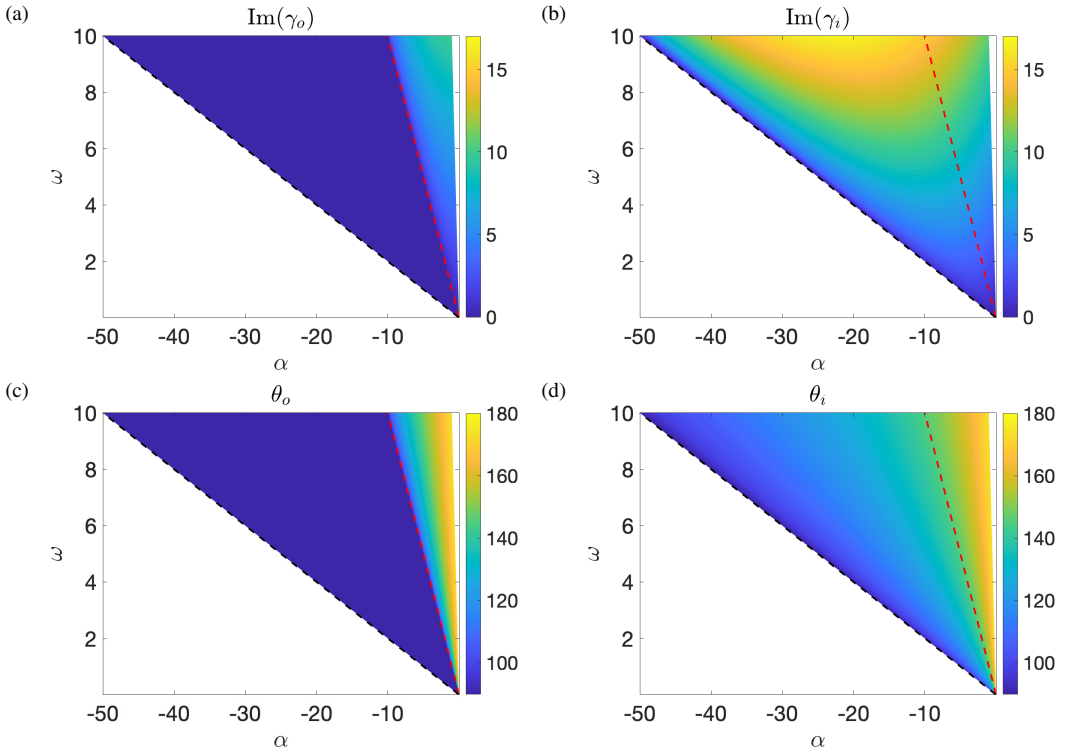

Fig. 6 Imaginary part of the coefficients $\gamma_{i,o}$ and their associated propagation angle for upstream-travelling waves generated in the flow region. Red dashed lines: $\alpha = -\omega$. Black dashed lines: $\alpha = -\omega/(\sqrt{T} - M)$. Results for $M = 0.8$, $T = 1$.

As before, information regarding wave amplitude is contained within the reflection and transmission coefficients. The magnitudes of the reflection coefficient for incidence angles at which waves are oscillatory in the quiescent medium are somewhat similar to those observed in figure 5; outside that band of phase velocities, however, the reflection coefficient has unit magnitude for all angles, characteristic of the total-reflection mechanism studied in Keller [54], Miles [55]. At the sonic line $\alpha = -\omega$, the reflection coefficient is 1, leading to a transmission coefficient of 2 – this is the last wavenumber that leads to oscillatory waves in the quiescent region, which assumes the shape of a planar wave going directly upstream. Note that the resulting transmitted wave has maximum amplitude for that value of α; for $\alpha < -\omega$, the magnitude of the transmission coefficient decreases rapidly. This indicates that, in addition to being y-decaying, the amplitude of the wave in the quiescent region even at positions very close to the shear layer decreases as the magnitude of α is increased.

An illustration of what happens close to the sonic line is shown in figure 8, for $c = \omega/\alpha = -1.01$, -1 and -0.99. For supersonic disturbances ($c = \omega/\alpha < -1$), the transmitted wave is oscillatory at an angle (in this case, $c = -1.01$ is close to 90°). In the flow region, a constructive/destructive interference pattern is observed, but with a significantly stronger contribution from the incident wave. At $c = -1$, the transmitted wave in the quiescent medium travels perpendicularly to the shear layer, and a standing wave pattern is observed in the flow region. This pattern remains basically unchanged as c increases further, but the transmitted wave for these values of phase velocity decays exponentially with distance from the shear layer.

To clarify the behaviour of the scattered pressure field as a function of the incidence angle, its absolute value as a function of the phase velocity c is shown in figure 9 for $\omega = 1$. In this plot, $c < -1$ ($\alpha > -1$) indicates supersonic

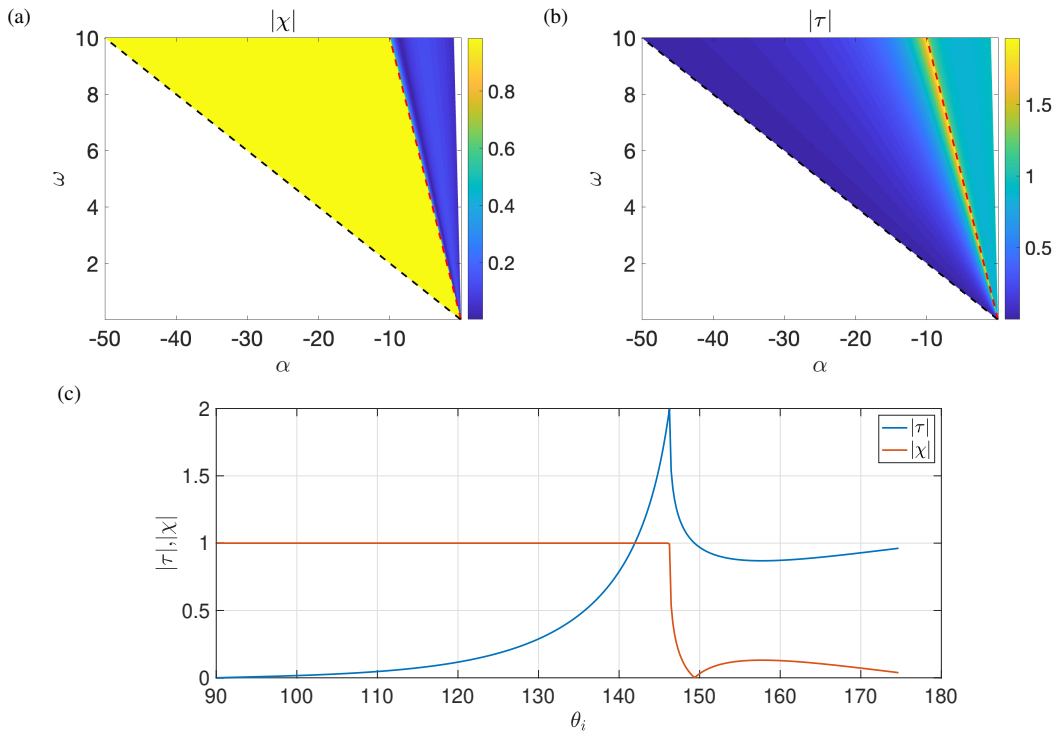

Fig. 7 Absolute value of reflection and transmission coefficients for upstream-travelling waves generated in the flow region for $M = 0.8$ and $T = 1$. Coefficients shown as a function of α and ω (a,b) and as a function of the flow medium wave incidence angle θ_i.

(propagating in the quiescent region) wavenumbers, while $c > -1$ ($\alpha < -1$) indicates waves that are oscillatory inside and decaying outside. It is clear that, while the pressure amplitude (and the equivalent acoustic energy) is somewhat uniformly distributed in the entire domain for the supersonic region, this amplitude in the flow region is considerably larger for $c > -1$. In fact, if this flow region is considered as a surrogate of the inside of a planar jet, this suggests that incidence angles associated with y-decaying behaviour in the quiescent region may lead to the highest flow response. Keeping in mind that energy is not conserved in the scattering problem, this is still in-line with the expected physical behaviour for these systems: as the wave is totally trapped, energy cannot escape from the flow region, leading to high flow responses.

C. Linking the scattering problem to the linear stability problem

As shown in Gojon et al. [58], the guided-jet mode for the DVS exists only at select frequencies, and for these frequencies only at subsonic phase velocities $\alpha \leq -\omega$. It presents a decaying behaviour in the quiescent region, while being energetic and displaying a standing-wave-like behaviour in the flow region. These are all characteristics shared by the current scattering model when considering waves originating in the flow region, despite the absence of a second shear layer. These observations suggest that the guided-jet mode might be a result of transmission and reflection of acoustic waves generated within the flow, as assumed in Towne et al. [10] and Martini et al. [49]. The transmitted component manifests as a subsonic wave in the quiescent region, similar to the surface waves explored in Rienstra and Hirschberg [51]. However, so far the model does not capture one of the most important characteristics of the guided-jet mode, which is the finite bands of frequency where it exists as a neutral wave in the eigenspectrum. In fact, in the scattering problem, guided-jet-like waves exist for a wide range of wavenumbers for a given frequency, between phase velocities associated with perpendicular waves in the quiescent and flow regions.

A stronger connection between the guided-jet mode and the current model may be obtained by considering the standing-wave behaviour in the flow region. As shown in figure 9, the most marked characteristic of the resulting wave as the phase velocity becomes subsonic is the presence of a standing wave in the y-direction, with $|\chi_i| = 1$. With the magnitude of the reflection coefficient at unity, the value of the reflection coefficient may be represented only in terms of

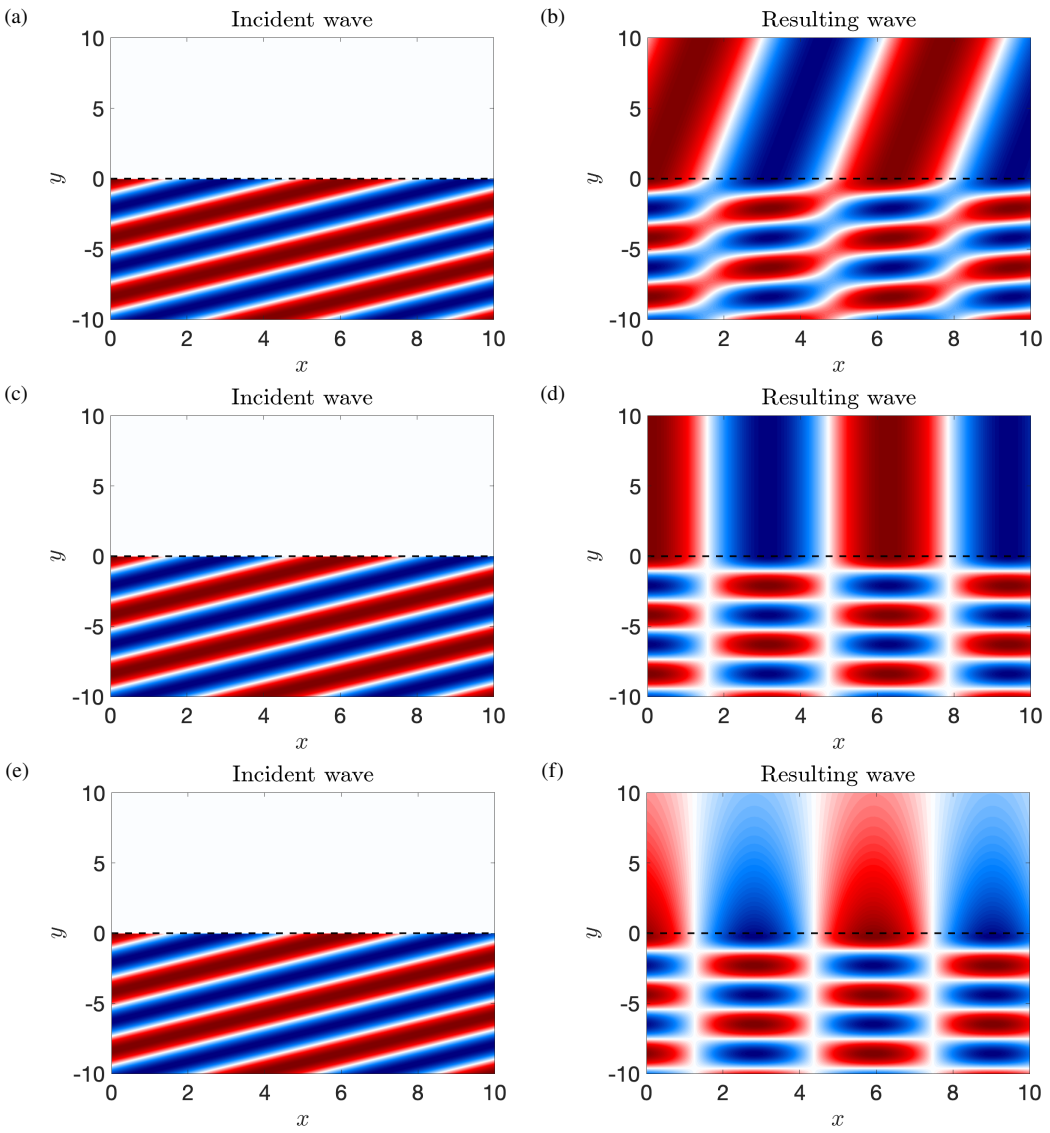

Fig. 8 Real part of pressure for the incident (a,c,e) and resulting fields after scattering (b,d,f). Results are shown for incidence angles associated with $c = \omega/\alpha = -1.01$ (a,b), -1 (c,d) and -0.99 (e,f) for $M = 0.8$ and $T = 1$.

its phase $\chi_i = \mathrm{e}^{\mathrm{i}\phi}$, with $-\pi \leq \phi < \pi$, and the resulting pressure field in the flow region may be represented as

$$p_i(y) = \mathrm{e}^{\gamma_i y} + \mathrm{e}^{\mathrm{i}\phi}\mathrm{e}^{-\gamma_i y} = 2\mathrm{e}^{\mathrm{i}\phi/2}\cos\left(\gamma_i y/\mathrm{i} - \phi/2\right). \tag{25}$$

The dependence of p on the cosine of y in the above expression highlights the standing-wave behaviour of the pressure in the flow region. Note that (25) is an alternative way to write the dispersion relation presented in Section II.A.2, which is now broken into individual pieces.

To connect this behaviour to what is observed in jets requires the imposition of an additional condition: the wavelength of the pressure standing wave in the flow region must be matched to the width of the jet to account for the symmetry of the problem, as symmetry or anti-symmetry can only be imposed if an integer number of half-wavelengths fit within the bounds of the jet. Mathematically, if the jet has width h, this is equivalent to solving

$$\cos\left(-\gamma_i h/\mathrm{i} - \phi/2\right) = \pm\cos\left(-\phi/2\right), \tag{26}$$

where the $\pm$ signs indicate symmetric and anti-symmetric modes, respectively. Each symmetry has two possible

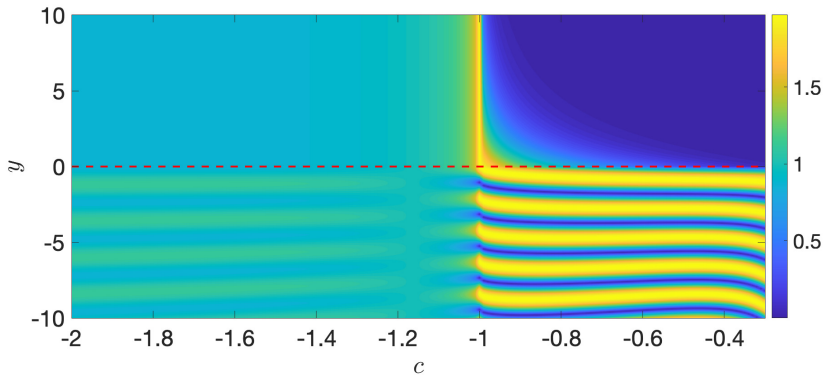

Fig. 9 Absolute value of pressure of the resulting field as a function of the phase velocity c for $\omega = 1$, $M = 0.8$ and $T = 1$.

solutions,

$$\gamma_i h/\mathrm{i} = -\phi + 2n\pi \tag{27}$$

for symmetric modes and

$$\gamma_i h/\mathrm{i} = -\phi + (2n+1)\pi \tag{28}$$

for antisymmetric modes, where n is an integer (another solution for each symmetry may be obtained if ϕ is set as zero, which will also be considered shortly). Considering ϕ a free parameter, these equations may solved directly, leading to

$$\omega = M\alpha \pm \sqrt{T}\sqrt{\alpha^2 + (k\pi - \phi)^2}. \tag{29}$$

Here, the integer k replaces n in (27)-(28), with symmetric/anti-symmetric modes being associated with even/odd values of k. The integer k must also be positive to ensure positive values for γ_i. The $\pm$ in (29) represents the two possible frequencies in the problem, but only the solution associated with the positive sign leads to positive frequencies for negative streamwise wavenumbers. Also note that the factor h was incorporated in the normalisation of α and ω in the current expression.

Equation (29) is precisely the dispersion relation of a planar duct with an assumed impedance at the wall [51]; the limiting cases $\phi = -\pi$ and $\phi = 0$ are associated with soft- ($p = 0$) (impedance $Z = 0$) and hard-wall ($\partial p/\partial y = 0$) $|Z| = \infty$ boundary conditions. Any value of impedance in-between these values may be represented by the reflection phase ϕ. The same equation may be used to predict the frequency-wavenumber pairs for which the standing wave in the scattering problem would fit inside of a jet of height h. This may be done by finding the values of (ω, α) for which the phase of the reflection ϕ satisfies (29). This solution is depicted by the red squares in figure 10, for both the symmetric and anti-symmetric modes at $M = 0.8$ and $M = 1.2$. In the same figure, the soft- and hard-wall duct dispersion relations are plotted, as well as the guided-jet mode solution obtained from the DVS. It is clear that the behaviour of the mode for higher magnitudes of α is well captured by the soft-wall duct dispersion relation, a result also observed in Towne et al. [10] for circular jets. However, the key new result here is that the branch point (which must occur at the line $\alpha = -\omega$) of the guided-jet mode is bound by the hard-wall duct dispersion relation; the intersection between this dispersion relation and the sonic line matches the DVS branch point perfectly. It is worth noting that this trend is also similar to the one identified in Martini et al. [49] when studying downstream-travelling supersonic modes, suggesting that hard-walled duct behaviour is usually found for $|c| = 1$ for modes of similar nature. Finally, the comparison between results from the DVS and the dispersion relation obtained from the standing-wave argument leads to a perfect match, providing final proof that, at least in a planar jet, wave reflection and transmission underpin the structure known as the guided-jet mode.

As the solution at the branch point is associated with a hard-wall boundary condition, a closed expression for that point may be obtained from the dispersion relation. After some algebra, the Strouhal numbers of the branch points for symmetric modes are found to be

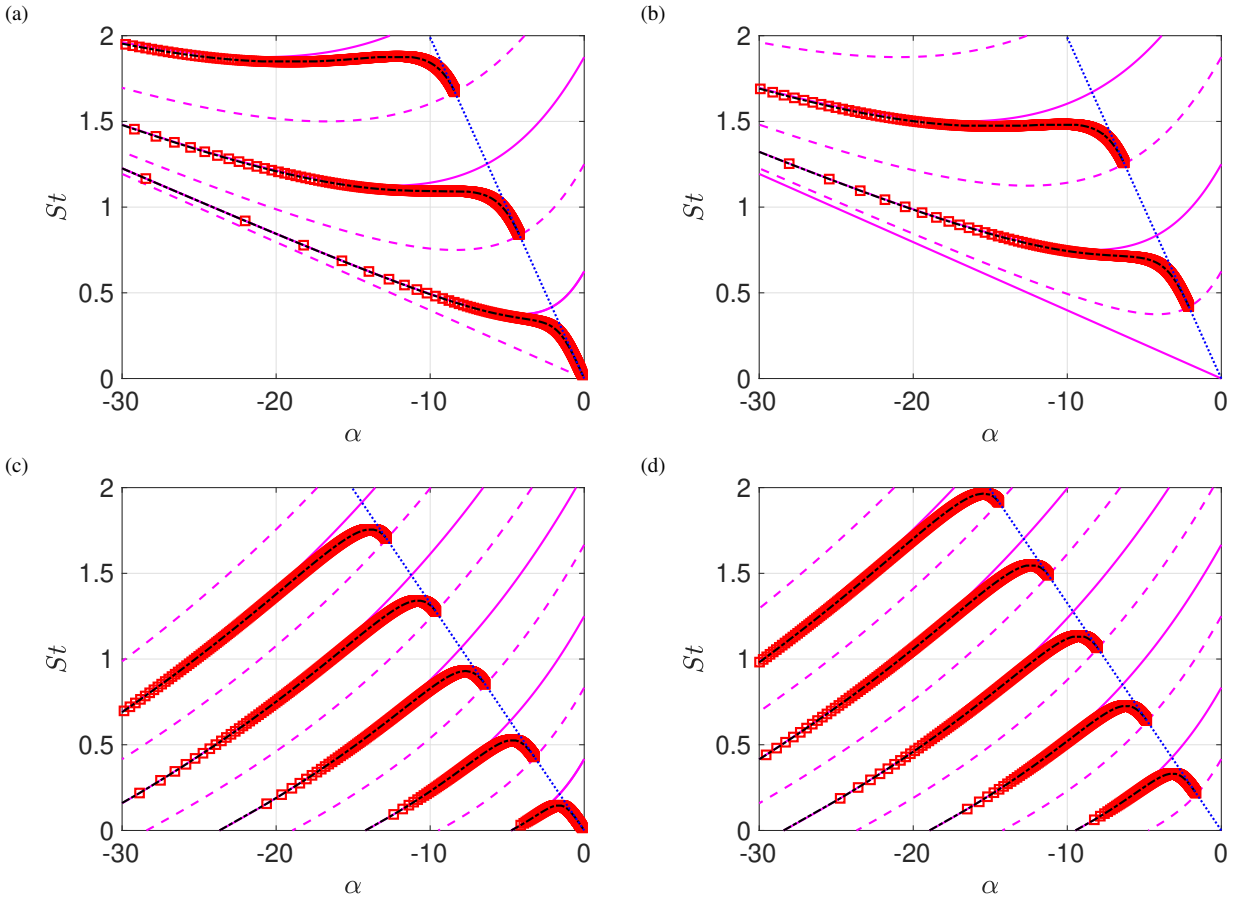

Fig. 10 Prediction of cut-on frequency-wavenumber pairs of totally reflected acoustic waves based on the wavelength of standing waves. Solution for symmetric (a,c) and anti-symmetric (b,d) modes for $M = 0.8$ (a,b) and 1.2 (c,d), with $T = 1$. Dotted (..) blue lines indicate the sonic line, magenta solid (-) and dashed (- -) lines indicate the soft- and hard-wall duct dispersion relations, black dash-dot (-.-) lines indicate the guided-jet mode obtained from the DVS dispersion relation and red squares (□) show the frequencies obtained from the standing wave argument using the SVS.

$$St_{br,S} = \frac{2n}{2M\sqrt{\frac{(M+1)^2}{T} - 1}} \tag{30}$$

and, for anti-symmetric modes,

$$St_{br,A} = \frac{2n+1}{2M\sqrt{\frac{(M+1)^2}{T} - 1}}, \tag{31}$$

where n is a non-negative integer. One should note that no branch point is recovered if $M < \sqrt{T} - 1$. This is to be expected, as total reflection only occurs for $\alpha = -\omega$ and $-\omega \geq \alpha \geq -\omega/(\sqrt{T} - M)$ – no value of α is within this interval for $M < \sqrt{T} - 1$. Figure 11 shows the behaviour of St_{br} as a function of Mach number, which is in line with results from the literature [58]. These are also the equivalent forms of the expressions obtained by Tam and Norum [33] for a planar jet, derived by simply replacing $\alpha = -\omega$ in the DVS dispersion relation.

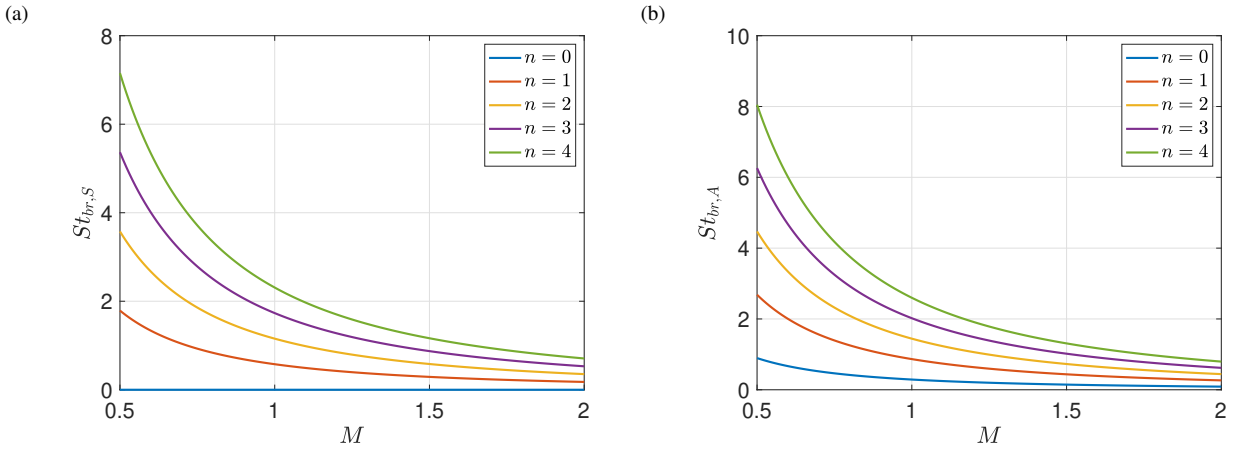

Fig. 11 Branch points for the symmetric (a) and anti-symmetric (b) solutions and $T = 1$ as a function of Mach number. Note that the first symmetric branch point is at zero frequency.

IV. Wave propagation and energy flux

The analysis in the previous section provides insight about the dynamics of the guided-jet mode, including the location where it is generated, its spatial support and a reasoning for its discrete frequency-wavenumber behaviour. However, it does not provide any explanation for its direction of propagation. The guided-jet mode may be defined as the upstream-travelling part of the neutral discrete waves supported by a jet at negative wavenumbers; if one follows each branch of the dispersion relation, it is clear that, depending on the Mach number, waves belonging to that branch could be either upstream- or downstream-travelling. We now proceed to uncover why this change in direction of propagation occurs.

Considering first the part of the wave that is transmitted to the quiescent medium, for the range of incidence angles considered in this work, it is straightforward to see that any transmitted wave will travel upstream ($90° \leq \theta_o \leq 180°$). Even for the waves with subsonic phase speed in the axial direction, there is no mechanism by which acoustic waves in the quiescent region can produce a downstream propagation of energy. This is not true in the flow region. Recalling that planar waves are defined in the frame of reference of the stream, in the frame of reference at rest, waves impinging directly on the shear layer ($\theta_i = 180°$) must be convected downstream. On the other hand, for subsonic Mach numbers, waves travelling perpendicular to the shear ($\theta_i = 90°$) will carry energy in the upstream direction. The angle at which the transition between upstream and downstream transport of energy occurs can be obtained by rewriting the velocity of the wave in the stationary frame of reference:

$$v_x = \sqrt{T}[M - \sin(\pi - \theta_i)]. \tag{32}$$

The phase velocity associated with zero streamwise velocity is then given by

$$c_0 = M - \sqrt{T(b^{-2} + 1)}, \tag{33}$$

with

$$b = \tan(\pi - \text{asin}M). \tag{34}$$

The expression above defines the minimum phase velocity of acoustic waves that carry energy in the upstream direction; if $c < c_0$ (or $\alpha > \omega/c_0$), the wave will transport energy in the downstream direction. This value of phase velocity is also the one associated with saddle points predicted in the spatial analysis of planar ducts (similar to Towne et al. [10], Rienstra and Hirschberg [51]).

A. Energy Flux

To quantify the transport of energy by these waves, a streamwise energy flux (or intensity) $I_{x,i}$ per unit z may be defined in the same fashion as in Rienstra and Hirschberg [51], which can be rewritten consistent with the current normalisation as

$$I_{x,(i,o)} = \int \frac{1}{T_{i,o}} \mathrm{Re}\left[(1+M_{i,o}^2)p_{i,o}u_{i,o}^* + M_{i,o}u_{i,o}u_{i,o}^* + M_{i,o}p_{i,o}p_{i,o}^*\right] dy, \tag{35}$$

where the superscript * indicates the complex conjugate, which leads to a real-valued energy flux. Here, this flux is integrated between $y = -h/2$ and 0 (or half the width of a planar jet) in the flow region, and between $y = 0$ and ∞ in the quiescent region. The integration limits are defined considering the symmetry of the problem, so as to provide a clearer connection to the planar-jet problem. It is important to note that the flux is not a well-defined quantity in linearised acoustics [59], and it can only provide an approximation of the direction energy is carried in the flow. Eigen-analysis of these flows leads to modes (frequency-wavenumber pairs associated with different waves in the flow) that carry energy in the upstream or downstream directions; the propagation direction in this case is well defined by the Briggs-Bers criterion [60]. Modes are not defined in the scattering problem, but it may be expected that equation 35 provide a good approximation for the energy flux associated with each frequency-wavenumber pair, at least if waves are acoustic-like and neutrally stable.

We start the analysis with the different flux components for the $M = 0.8$ case. Figure 12 shows the flux obtained from (35) in both the quiescent (a) and flow (b) regions. As expected, the energy flux is negative in the quiescent region as the energy is transported in the direction of propagation of the wave; there is no mechanism by which this wave could transport energy downstream in this region. The flux magnitude in the quiescent region is maximum at the sonic line ($\alpha = -\omega$), which is due to two factors. First, the transmission coefficient is maximum at this point, which naturally increases the flux. The second (and more important) factor is that the wave is oscillatory at the sonic line, and becomes progressively more decaying in the y-direction as its phase velocity decreases in magnitude. Given the integration is performed between the shear layer and infinity, the damping of the wave with increasing distance from the shear layer means the contribution of these perturbations to the integral (35) becomes vanishingly small as the wave becomes increasingly more confined.

In the flow region, the behaviour of the flux is qualitatively different, as shown in figure 12b. The flux may be positive or negative depending on the angle of propagation of the wave, with the propagation angle that produces no net-energy propagation indicated with the dashed red line. For wavenumbers to the left of the red line (blue region of the plot), the energy flux is negative and energy is transported in the upstream direction. As the incidence angles steepens (or as α increases in magnitude), more and more energy is transmitted in the upstream direction, which is in line with the expected physical behaviour for these acoustic waves. The equivalent behaviour is observed for wavenumbers to the right of the red line (red region), where energy is transported downstream; the wave is convected by the flow.

Since the flux in the flow and quiescent regions may have different signs depending on the propagation angle, the frequency-wavenumber space may be divided into three distinct zones, based on contribution of each region to the overall flux and the resultant direction of net energy propagation. This is shown as $log(|I_{x,o}|/|I_{x,i}|)$ in figure 12c; magenta zones in these plots indicate that the energy flux is dominated by the quiescent region (which only carries energy upstream), and green zones indicate that the propagation of energy is dominated by the flow region (which may carry energy upstream or downstream). In this plot, it is clear that the quiescent region dominates the energy flux for waves with phase velocity close to the quiescent-region speed of sound (zone 1). The behaviour as streamwise wavenumber becomes more negative is not monotonic, with three zero crossings and one discontinuity. The most complex behaviour is evident in zone 2, which exhibits the following trends with reductions in the magnitude of streamwise phase velocity: first, the relative contribution of the quiescent region to the total flux reduces until the first zero crossing is reached, at which point the regions contribute equally. With further reduction, the contribution from the flow region decreases until it reaches another minimum; though the fluxes in both regions are reducing, the reduction is more rapid in the flow stream. This then leads to a second zero crossing, before the ratio becomes discontinuous as the phase velocity corresponding to no energy propagation ($c = c_0$) in the flow region is reached. From this point onwards, the trends are monotonic, with one final point of equal contribution before the flow region increasingly dominates as phase velocity reduces in magnitude; this monotonic region is referred to as zone 3.

To produce a final explicit link between the results of the acoustic scattering problem and the dispersion relation of the vortex sheet, we consider the total net flux across the entire integration region. A comparison between this total flux and the dispersion relation of the guided-jet modes is shown in figure 12d. The group velocity of the discrete waves predicted by the DVS are in close agreement with the values of flux computed in the scattering problem; whenever the slope is negative (associated with upstream-travelling waves), the mode is found to be in the blue region of the plot, while positive-group-velocity waves are co-located with positive (downstream) energy flux. The magnitude of the phase velocity also follows the strength of the flux computed by the model. The comparison is not perfect; when the flux is very close to zero the scattering problem and the DVS predict slightly different points of zero group velocity.

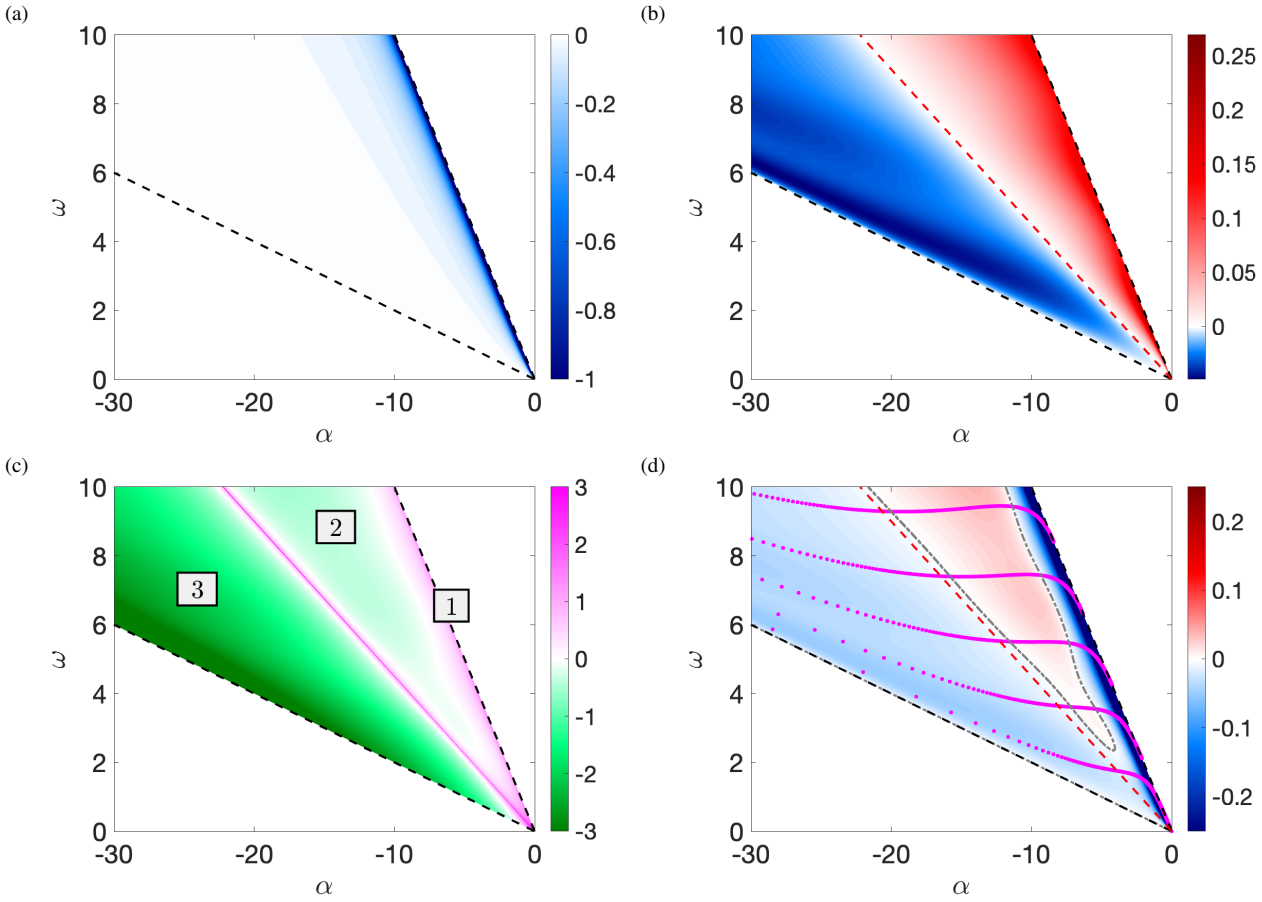

Fig. 12 Streamwise energy flux for waves travelling in the quiescent region (a) and flow region (b) as a function of frequency and wavenumber for $M = 0.8$. Logarithm of the absolute value of the ratio between the fluxes (c) and the total energy flux (d) are also shown. Black dashed lines indicate wavenumber-frequency pairs where total reflection occurs, and the red dashed line indicates the phase speed associated with no energy propagation in the streamwise direction. Grey dot-dashed lines indicate regions where the flux is zero, and magenta dots represent the dispersion relation of the guided-jet mode.

Nonetheless, this result not only reinforces the link between the two models, but also provides a lens through which to understand the behaviour of the guided-jet mode: changes in the group velocity of the guided-jet mode can be linked to changes in the total energy flux between the jet and its environment.

B. The effect of Mach Number

As detailed in Towne et al. [10], the guided-jet mode exhibits a complicated dependence on Mach number. Additionally, one of the least intuitive aspects of this mode is that it can transport energy upstream in a supersonic jet, despite having peak amplitudes within the supersonic core of the flow. We now consider the effect of Mach number, with four values chosen to span the range over which the guided-jet mode exhibits qualitative changes in behaviour, as shown in figures 13 (for the flow-region flux) and 14 (for the total flux, with the results of the DVS superposed). The behaviour in the quiescent region remains qualitatively the same as a function of M and is omitted for brevity. For sufficiently low Mach number, the phase speed associated with stationary waves in the flow ($c = c_0$, the dashed red line in figure 12) is located to the right of the sonic line, meaning that all subsonic waves are upstream travelling. This is exemplified in figure 13a for $M = 0.6$. As such, for any incident wave with an upstream component, the resultant total-energy flux must be negative; no downstream-travelling waves can be produced in this region at this Mach number for upstream-travelling incident waves. This is confirmed by the results of the DVS in figure 14a; all discrete modes are upstream-travelling for this case [see also 53]. As the Mach number increases, the line $\omega/\alpha = c_0$ crosses the

sonic line, allowing for downstream-travelling disturbances in the flow region to be produced by the interaction of upstream-propagating waves with the shear layer for this rage of frequencies and wavenumbers. Increasing M further decreases the slope of the $\omega/\alpha = c_0$ line, increasing the size of the parameter space where downstream-travelling waves are allowed, while constricting the values of ω and α that correspond to negative energy flux. Finally, at supersonic Mach numbers, no upstream-travelling wave is allowed within the flow, and all waves in the flow will transfer energy in the downstream direction. This is an entirely expected result, as no acoustic perturbation can propagate in the upstream direction (in a frame of reference at rest) in a supersonic flow.

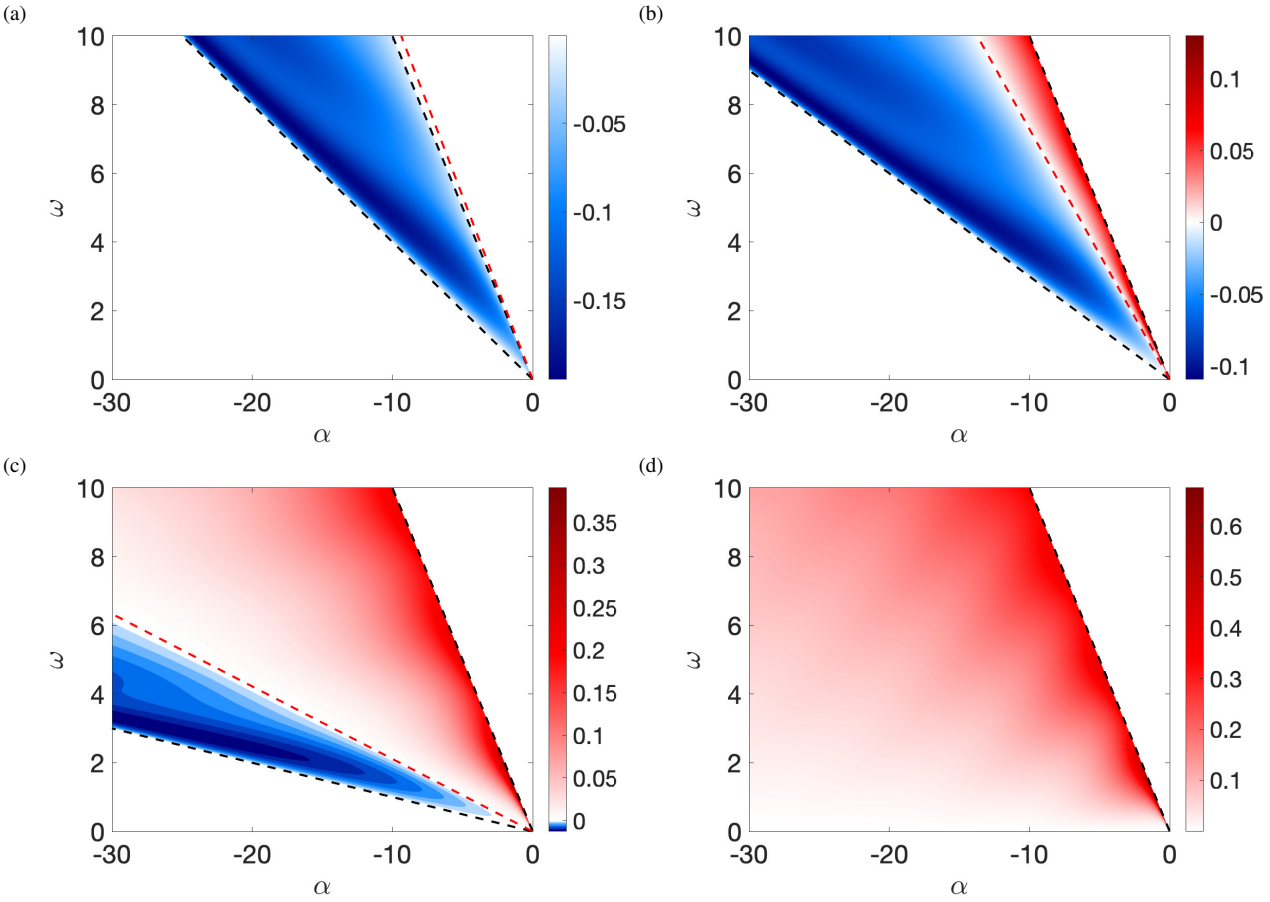

Fig. 13 Streamwise energy flux for waves travelling in the flow region, integrated between $y = -h/2$ and 0 as a function of frequency and wavenumber for $M = 0.6$ (a), $M = 0.7$ (b), $M = 0.9$ (c) and $M = 1.2$ (d). Black dashed lines indicate the region where total reflection occurs, and the red dashed line indicates the phase speed associated with no energy propagation in the streamwise direction.

Considering the propagation of waves in the flow region offers some insight into the behaviour of the guided-jet mode, particularly in the region $0.8 \leq M < 1$. The total flux, as presented in figure 14 can be examined to provide insight on the broad role of the guided-jet mode. The gray lines in this figure indicate regions where the fluxes in both regions are the equal in magnitude and opposite in direction. These indicate regions where the total energy of the wave does not travel in either direction – or the energy flux in the quiescent region is perfectly counterbalanced by the one in the flow region. Inspection of figure 14 shows that these gray lines are very close to the position of the saddle points of the guided-jet and duct-like modes, but they do not match perfectly. The reason for this slight mismatch is not clear, but one possibility is that the definition of energy flux given in Rienstra and Hirschberg [51] (which considers acoustic homentropic disturbances and uniform flow) may not be the most appropriate choice for the description of the present phenomenon [59, 61]. Still, the energy fluxes provide a very good first approximation of the saddle points and the direction of propagation of the different waves in the flow, indicating that the upstream energy flux of the quiescent medium is a key ingredient of the physics of this mode.

The flux analysis provides the final piece of the guided-jet mode puzzle. It shows that the direction of propagation of the discrete waves with negative phase velocity from the spatial Navier-Stokes spectrum can be approximated by their energy flux, which can be defined in the context of an acoustic-scattering problem. This is the key to understand why the modes close to the acoustic line propagate in the upstream direction, even in supersonic jets; due to the large outreach and high transmission coefficient of the transmitted wave in the quiescent medium, its energy flux is so strong for those wavenumbers that it overcomes the flux magnitude of the wave inside of the jet, which carries energy downstream. It also explains the presence of different neutral saddle points in the spectrum, which are associated with a change in flux direction; a change in flux also leads to a change in group velocity of the wave. Finally, the analysis of the flux also explains the behaviour of the guided-jet and duct modes as a function of Mach number, as the flux in the flow region changes considerably with that parameter.

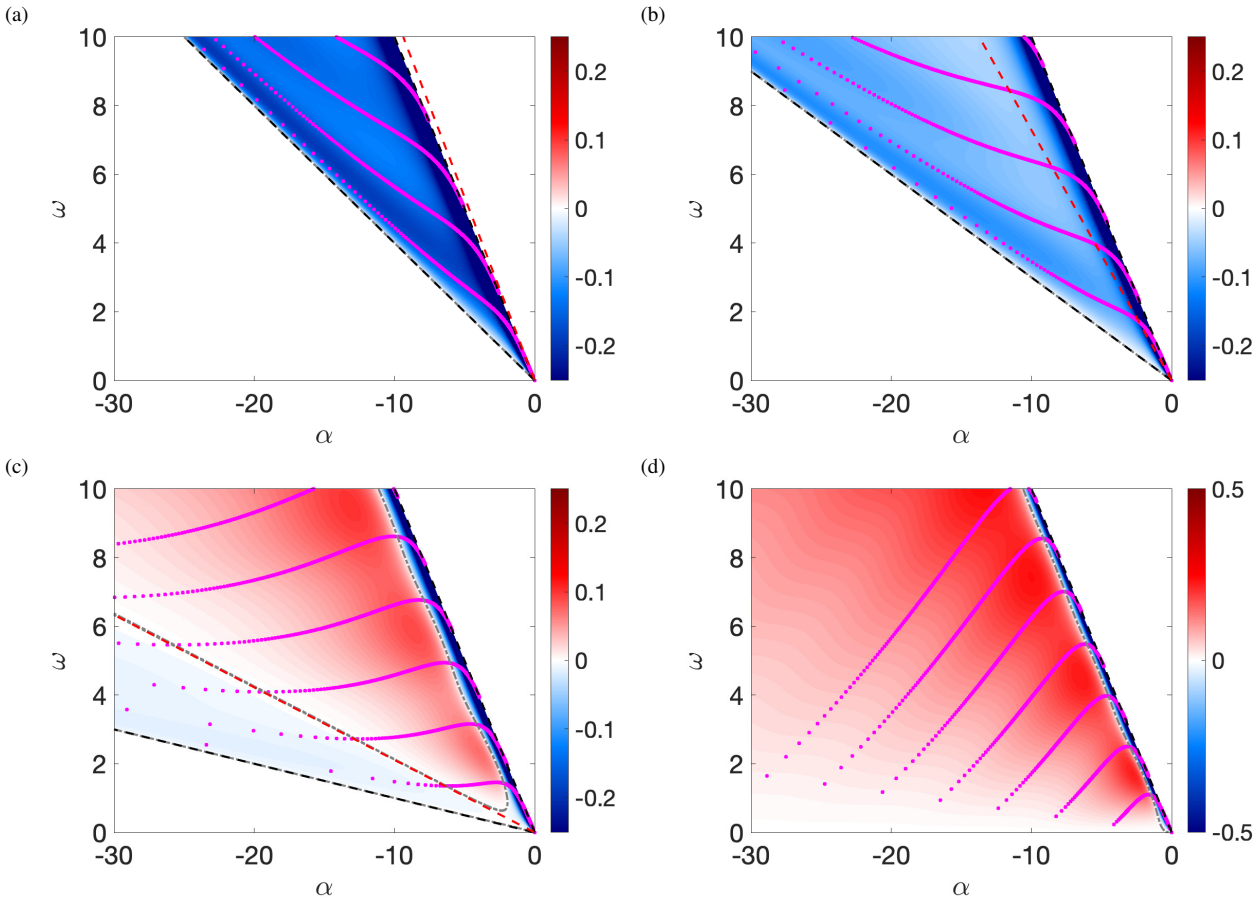

Fig. 14 Total energy flux as a function of frequency and wavenumber for $M = 0.6$ (a), $M = 0.7$ (b), $M = 0.9$ (c) and $M = 1.2$ (d). Black dashed lines indicate the frequency and wavenumber pairs where total reflection occurs, and the red dashed line indicates the phase speed associated with no energy propagation in the streamwise direction in the flow region. Grey dash-dot lines indicate the frequency/wavenumber pairs where the flux is zero. The magenta dots indicate the frequencies and wavenumbers of the guided-jet mode.

V. Conclusions

In the present work, the behaviour of discrete modes with negative phase velocity (namely the guided-jet mode and duct-like modes) in the linearised Navier-Stokes spectrum was analysed by connecting it with an acoustic-scattering problem. Recent works have highlighted the importance of these modes in a myriad of resonance phenomena including screech [37–39, 41], impingement/edge tones [32, 33, 53], and high-subsonic jet resonance [10]. However, the nature of this mode and a clear explanation for its behaviour as a function of frequency have not been expounded.

Analysis of the scattering problem with waves originating in the quiescent region reveals that there is no mechanism through which a planar wave travelling directly upstream can be transmitted to the flow region, precluding the generation of patterns such as that associated with the guided-jet mode. On the other hand, waves generated in the flow region can experience total reflection for a range of frequencies and wavenumbers, and the range of frequency and wavenumber pairs over which this occurs matches the range for which discrete modes are observed in the planar-jet vortex sheet. In this range, the phase of the reflection determines the wavelength of the standing wave formed in the flow region. Even though the reflection coefficient is unitary in this range, maximum transmission is observed when disturbances are sonic (despite the fact that disturbances in the quiescent region are decaying, as highlighted by Keller [54]); the transmission coefficient then rapidly decreases as this wave becomes more and more subsonic, leading to mode structures confined to the flow region, which assume the shape of a standing wave in y. By imposing a requirement that this structure must match with the width of a planar jet, the dispersion relation of the discrete modes is recovered perfectly.

To obtain the direction of propagation of the resulting wave, the energy flux in the streamwise direction was calculated and compared with the dispersion relation obtained from the double-vortex-sheet model. It was shown that, at frequency-wavenumber pairs close to the sonic line, the energy flux is dominated by the quiescent region direction (a consequence of high transmission values in this regime), with increases in wavenumber producing a concomitant increase in the flux associated with the flow region. Depending on the Mach number, both upstream- and downstream-travelling waves are obtained from the flux calculation, which closely match the behaviour of the group velocity of the discrete modes from the vortex-sheet model. The frequency-wavenumber pairs for which the net flux over both regions is zero closely approximate the saddle points from the vortex-sheet model.

These results altogether suggest that the discrete modes in the negative part of the Navier-Stokes spectrum are of acoustic origin, with the particularity that disturbances are totally reflected (or trapped) inside of the jet. For high wavenumbers, this trapped wave has no support in the quiescent region, with the jet behaving almost like a soft duct. However, for wavenumbers close to the sonic line, the amplitude of the transmission is strong, but the wave is nonetheless evanescent/decaying in y. Even though it decays exponentially in y, this wave still carries significant amounts of energy in the upstream direction, critical to the function of the guided-jet mode in closing resonance. The current results builds upon the work of Martini et al. [49] in unifying the different eigenvalues in the negative-wavenumber half-plane previously studied by Tam and Hu [34] and Towne et al. [10] under a single label: acoustic duct-like modes. While they seem to share the same nature, details such as direction of propagation, transmission rate and spatial support are defined by their streamwise wavenumber and the other physical parameters of the problem, such as Mach number and temperature ratio.

Acknowledgments

This work was sponsored by both the Australian Research Council through the Discovery Project scheme (DP220103873) and the Office of Naval Research (ONR), under grant number #N00014-22-1-2503. The views and conclusions contained herein are those of the authors only and should not be interpreted as representing those of ONR, the U.S. Navy or the U.S. Government.

References

[1] Berndt, D., "Dynamic pressure fluctuations in the internozzle region of a twin-jet nacelle," Tech. rep., SAE Technical Paper, 1984.

[2] Powell, A., "The Noise of Choked Jets," *The Journal of the Acoustical Society of America*, Vol. 25, No. 3, 1953, pp. 385–389. https://doi.org/10.1121/1.1907052.

[3] Raman, G., "ADVANCES IN UNDERSTANDING SUPERSONIC JET SCREECH: REVIEW AND PERSPECTIVE," *Progress in Aerospace Sciences*, Vol. 34, No. 1, 1998, pp. 45 – 106. https://doi.org/https://doi.org/10.1016/S0376-0421(98)00002-5, URL http://www.sciencedirect.com/science/article/pii/S0376042198000025.

[4] Edgington-Mitchell, D., "Aeroacoustic resonance and self-excitation in screeching and impinging supersonic jets – A review," *International Journal of Aeroacoustics*, Vol. 18, No. 2-3, 2019, pp. 118–188. https://doi.org/10.1177/1475472X19834521.

[5] Marsh, A. H., "Noise measurements around a subsonic air jet impinging on a plane, rigid surface," *The Journal of the Acoustical Society of America*, Vol. 33, No. 8, 1961, pp. 1065–1066.

[6] Wagner, F., *The sound and flow field of an axially symmetric free jet upon impact on a wall*, National Aeronautics and Space Administration, 1971.

[7] Powell, A., "The sound-producing oscillations of round underexpanded jets impinging on normal plates," *The Journal of the Acoustical Society of America*, Vol. 83, No. 2, 1988, pp. 515–533.

[8] Henderson, B., "The connection between sound production and jet structure of the supersonic impinging jet," *The Journal of the Acoustical Society of America*, Vol. 111, No. 2, 2002, pp. 735–747.

[9] Henderson, B., Bridges, J., and Wernet, M., "An experimental study of the oscillatory flow structure of tone-producing supersonic impinging jets," *Journal of Fluid Mechanics*, Vol. 542, 2005, pp. 115–137.

[10] Towne, A., Cavalieri, A. V. G., Jordan, P., Colonius, T., Schmidt, O., Jaunet, V., and Brès, G. A., "Acoustic resonance in the potential core of subsonic jets," *Journal of Fluid Mechanics*, Vol. 825, 2017, p. 1113–1152. https://doi.org/10.1017/jfm.2017.346.

[11] Schmidt, O. T., Towne, A., Colonius, T., Cavalieri, A. V. G., Jordan, P., and Brès, G. A., "Wavepackets and trapped acoustic modes in a turbulent jet: coherent structure eduction and global stability," *Journal of Fluid Mechanics*, Vol. 825, 2017, p. 1153–1181. https://doi.org/10.1017/jfm.2017.407.

[12] Rayleigh, L., "On the stability, or instability, of certain fluid motions," *Proc. London Math. Soc.*, Vol. 9, 1880, pp. 57–70.

[13] Lessen, M., Fox, J. A., and Zien, H. M., "The instability of inviscid jets and wakes in compressible fluid," *Journal of Fluid Mechanics*, Vol. 21, No. 01, 1965, pp. 129–143.

[14] Michalke, A., "On the inviscid instability of the hyperbolic tangent velocity profile," *Journal of Fluid Mechanics*, Vol. 19, No. 04, 1964, pp. 543–556.

[15] Michalke, A., "On spatially growing disturbances in an inviscid shear layer," *J. Fluid Mech*, Vol. 23, No. 3, 1965, pp. 521–544.

[16] Mollo-Christensen, E., "Jet noise and shear flow instability seen from an experimenter's viewpoint(Similarity laws for jet noise and shear flow instability as suggested by experiments)," *Journal of Applied Mechanics*, Vol. 34, 1967, pp. 1–7.

[17] Crow, S. C., and Champagne, F. H., "Orderly structure in jet turbulence," *Journal of Fluid Mechanics*, Vol. 48, No. 3, 1971, pp. 547–591.

[18] Cavalieri, A. V. G., Rodríguez, D., Jordan, P., Colonius, T., and Gervais, Y., "Wavepackets in the velocity field of turbulent jets," *Journal of Fluid Mechanics*, Vol. 730, 2013, pp. 559–592. https://doi.org/10.1017/jfm.2013.346, URL http://journals.cambridge.org/article_S0022112013003467.

[19] Tinney, C., and Jordan, P., "The near pressure field of co-axial subsonic jets," *Journal of Fluid Mechanics*, Vol. 611, 2008, pp. 175–204.

[20] Cavalieri, A. V. G., Jordan, P., Colonius, T., and Gervais, Y., "Axisymmetric superdirectivity in subsonic jets," *Journal of Fluid Mechanics*, Vol. 704, 2012, p. 388.

[21] Jordan, P., and Colonius, T., "Wave Packets and Turbulent Jet Noise," *Annual Review of Fluid Mechanics*, Vol. 45, No. 1, 2013.

[22] Cavalieri, A. V. G., Jordan, P., Wolf, W. R., and Gervais, Y., "Scattering of wavepackets by a flat plate in the vicinity of a turbulent jet," *Journal of sound and Vibration*, Vol. 333, No. 24, 2014, pp. 6516–6531.

[23] Baqui, Y. B., Agarwal, A., Cavalieri, A. V. G., and Sinayoko, S., "A coherence-matched linear source mechanism for subsonic jet noise," *Journal of Fluid Mechanics*, Vol. 776, 2015, pp. 235–267.

[24] Cavalieri, A. V. G., Jordan, P., and Lesshafft, L., "Wave-Packet Models for Jet Dynamics and Sound Radiation," *Applied Mechanics Reviews*, Vol. 71, No. 2, 2019. https://doi.org/10.1115/1.4042736, URL https://doi.org/10.1115/1.4042736, 020802.

[25] Wong, M. H., Jordan, P., Maia, I. A., Cavalieri, A. V., Kirby, R., Fava, T. C., and Edgington-Mitchell, D., "Wavepacket modelling of broadband shock-associated noise in supersonic jets," *Journal of Fluid Mechanics*, Vol. 918, 2021, p. A9.

[26] Michalke, A., "Survey on jet instability theory," *Progress in Aerospace Sciences*, Vol. 21, 1984, pp. 159–199.

[27] Nogueira, P. A., and Edgington-Mitchell, D., "Investigation of supersonic twin-jet coupling using spatial linear stability analysis," *Journal of Fluid Mechanics*, Vol. 918, 2021, p. A38.

[28] Sinha, A., Rodríguez, D., Brès, G. A., and Colonius, T., "Wavepacket models for supersonic jet noise," *Journal of Fluid Mechanics*, Vol. 742, 2014, pp. 71–95. https://doi.org/10.1017/jfm.2013.660, URL http://journals.cambridge.org/article_S0022112013006605.

[29] Sasaki, K., Cavalieri, A. V. G., Jordan, P., Schmidt, O. T., Colonius, T., and Brès, G. A., "High-frequency wavepackets in turbulent jets," *Journal of Fluid Mechanics*, Vol. 830, 2017, p. R2. https://doi.org/10.1017/jfm.2017.659.

[30] Towne, A., and Colonius, T., "One-way spatial integration of hyperbolic equations," *Journal of Computational Physics*, Vol. 300, 2015, pp. 844–861.

[31] Nogueira, P. A., Self, H. W., Towne, A., and Edgington-Mitchell, D., "Wave-packet modulation in shock-containing jets," *Physical Review Fluids*, Vol. 7, No. 7, 2022, p. 074608.

[32] Tam, C. K., and Ahuja, K., "Theoretical model of discrete tone generation by impinging jets," *Journal of Fluid Mechanics*, Vol. 214, 1990, pp. 67–87.

[33] Tam, C. K., and Norum, T. D., "Impingement tones of large aspect ratio supersonic rectangular jets," *AIAA journal*, Vol. 30, No. 2, 1992, pp. 304–311.

[34] Tam, C. K. W., and Hu, F. Q., "On the three families of instability waves of high-speed jets," *Journal of Fluid Mechanics*, Vol. 201, 1989, p. 447–483. https://doi.org/10.1017/S002211208900100X.

[35] Oertel, H., "Mach wave radiation of hot supersonic jets investigated by means of a shock tube and new optical techniques," *Proceedings of the 12th International Symposium on Shock-Tubes and Waves, Israel*, 1980.

[36] Gojon, R., Bogey, C., and Marsden, O., "Investigation of tone generation in ideally expanded supersonic planar impinging jets using large-eddy simulation," *Journal of Fluid Mechanics*, Vol. 808, 2016, pp. 90–115.

[37] Gojon, R., Bogey, C., and Mihaescu, M., "Oscillation Modes in Screeching Jets," *AIAA Journal*, Vol. 56, No. 7, 2018, pp. 2918–2924. https://doi.org/10.2514/1.J056936.

[38] Edgington-Mitchell, D., Jaunet, V., Jordan, P., Towne, A., Soria, J., and Honnery, D., "Upstream-travelling acoustic jet modes as a closure mechanism for screech," *Journal of Fluid Mechanics*, Vol. 855, 2018, p. R1. https://doi.org/10.1017/jfm.2018.642.

[39] Mancinelli, M., Jaunet, V., Jordan, P., and Towne, A., "Screech-tone prediction using upstream-travelling jet modes," *Experiments in Fluids*, Vol. 60, No. 1, 2019, p. 22.

[40] Mancinelli, M., Jaunet, V., Jordan, P., and Towne, A., "A complex-valued resonance model for axisymmetric screech tones in supersonic jets," *Journal of Fluid Mechanics*, Vol. 928, 2021, p. A32.

[41] Nogueira, P. A. S., Jordan, P., Jaunet, V., Cavalieri, A. V., Towne, A., and Edgington-Mitchell, D., "Absolute instability in shock-containing jets," *Journal of Fluid Mechanics*, Vol. 930, 2022, p. A10.

[42] Nogueira, P. A. S., Jaunet, V., Mancinelli, M., Jordan, P., and Edgington-Mitchell, D., "Closure mechanism of the A1 and A2 modes in jet screech," *Journal of Fluid Mechanics*, Vol. 936, 2022, p. A10.

[43] Edgington-Mitchell, D., Li, X., Liu, N., He, F., Wong, T. Y., Mackenzie, J., and Nogueira, P., "A unifying theory of jet screech," *Journal of Fluid Mechanics*, Vol. 945, 2022, p. A8.

[44] Bogey, C., "Acoustic tones in the near-nozzle region of jets: characteristics and variations between Mach numbers 0.5 and 2," *Journal of Fluid Mechanics*, Vol. 921, 2021, p. A3.

[45] Bogey, C., "Tones in the acoustic far field of jets in the upstream direction," *AIAA Journal*, Vol. 60, No. 4, 2022, pp. 2397–2406.

[46] Zaman, K., Fagan, A., and Upadhyay, P., "Pressure fluctuations due to 'trapped waves' in the initial region of compressible jets," *Journal of Fluid Mechanics*, Vol. 931, 2022, p. A30.

[47] Weightman, J. L., Amili, O., Honnery, D., Edgington-Mitchell, D., and Soria, J., "Nozzle external geometry as a boundary condition for the azimuthal mode selection in an impinging underexpanded jet," *Journal of Fluid Mechanics*, Vol. 862, 2019, pp. 421–448.

[48] Varé, M., and Bogey, C., "Mach number dependence of tone generation by impinging round jets," *AIAA Journal*, 2023, pp. 1–15.

[49] Martini, E., Cavalieri, A. V. G., and Jordan, P., "Acoustic modes in jet and wake stability," *Journal of fluid mechanics*, Vol. 867, 2019, pp. 804–834.

[50] Campos, L., and Kobayashi, M., "On the reflection and transmission of sound in a thick shear layer," *Journal of Fluid Mechanics*, Vol. 424, 2000, pp. 303–326.

[51] Rienstra, S. W., and Hirschberg, A., "An introduction to acoustics," *Eindhoven University of Technology*, 2002.

[52] Crighton, D., and Leppington, F., "Radiation properties of the semi-infinite vortex sheet: the initial-value problem," *Journal of Fluid Mechanics*, Vol. 64, No. 2, 1974, pp. 393–414.

[53] Jordan, P., Jaunet, V., Towne, A., Cavalieri, A. V. G., Colonius, T., Schmidt, O., and Agarwal, A., "Jet–flap interaction tones," *Journal of Fluid Mechanics*, Vol. 853, 2018, p. 333–358. https://doi.org/10.1017/jfm.2018.566.

[54] Keller, J. B., "Reflection and transmission of sound by a moving medium," *The Journal of the Acoustical Society of America*, Vol. 27, No. 6, 1955, pp. 1044–1047.

[55] Miles, J. W., "On the reflection of sound at an interface of relative motion," *The Journal of the Acoustical Society of America*, Vol. 29, No. 2, 1957, pp. 226–228.

[56] Ribner, H. S., "Reflection, transmission, and amplification of sound by a moving medium," *The Journal of the Acoustical Society of America*, Vol. 29, No. 4, 1957, pp. 435–441.

[57] Ingard, U., "Influence of fluid motion past a plane boundary on sound reflection, absorption, and transmission," *The Journal of the Acoustical Society of America*, Vol. 31, No. 7, 1959, pp. 1035–1036.

[58] Gojon, R., Gutmark, E., and Mihaescu, M., "Antisymmetric oscillation modes in rectangular screeching jets," *AIAA Journal*, Vol. 57, No. 8, 2019, pp. 3422–3441.

[59] Morfey, C., "Acoustic energy in non-uniform flows," *Journal of Sound and Vibration*, Vol. 14, No. 2, 1971, pp. 159–170.

[60] Briggs, R. J., *Electron-stream interaction with plasmas*, No. 29 in Research Monograph, MIT Press, Cambridge, MA, 1964.

[61] Campos, L., and Kobayashi, M., "On an acoustic oscillation energy for shear flows," *International Journal of Aeroacoustics*, Vol. 12, No. 1-2, 2013, pp. 123–167.